APPLIED SCIENCES AND ENGINEERING

Soft and lightweight fabric enables powerful and high-range pneumatic actuation

Zhuang Zhang[1,2]†, Yongzhou Long[1]†, Genliang Chen[1,3]*, Qichen Wu[1], Hao Wang[1], Hanqing Jiang[2,4]*

Soft structures and actuation allow robots, conventionally consisting of rigid components, to perform more compliant, adaptive interactions similar to living creatures. Although numerous functions of these types of actuators have been demonstrated in the literature, their hyperelastic designs generally suffer from limited workspaces and load-carrying capabilities primarily due to their structural stretchability factor. Here, we describe a series of pneumatic actuators based on soft but less stretchable fabric that can simultaneously perform tunable workspace and bear a high payload. The motion mode of the actuator is programmable, combinable, and predictable and is informed by rapid response to low input pressure. A robotic gripper using three fabric actuators is also presented. The gripper demonstrates a grasping force of over 150 N and a grasping range from 70 to 350 millimeters. The design concept and comprehensive guidelines presented would provide design and analysis foundations for applying less stretchable yet soft materials in soft robots to further enhance their practicality.

INTRODUCTION

Inspired by the softness and natural compliance of biological systems, soft actuators and robots that are normally made of rubbery materials have been widely explored and demonstrated for various applications (e.g., locomotion, manipulation, and wearable and biomedical devices) (*1*–*10*) due to their attractive potential in human-robot interaction and complex environments (*11*). Among many actuation methods (e.g., electrical, thermal, optical, and magnetic) (*12*–*19*), pneumatic-driven soft actuators have garnered considerable attention for their simple and safe operation features, low cost, and ease of fabrication. These actuators comprise a cephalopod-liked structure entirely constructed from elastomeric materials (e.g., silicone rubber) and come equipped with pneumatic channels that provide various deformation modes upon pressure (*20*–*24*). Although these modes of deformation are dexterous and safe for interaction, their load-bearing and load-carrying capabilities are seriously compromised by the intrinsic stretchability of the rubbery materials. Several strategies have been explored to reach a balance between the two contradictory factors of being soft for human-friendly interaction and hard for load carrying, including directly incorporating high stiffness components [e.g., shells (*25*, *26*) and frames (*27*)] to form a hybrid system, constructing antagonistic actuation systems (*28*–*31*), and integrating other stiffness tunable materials/systems [e.g., jamming (*32*–*34*), low–melting point materials (*35*, *36*), shape memory polymers (*37*, *38*), electrorheological materials (*39*, *40*), and magnetorheological materials (*41*, *42*)]. Thus far, however, these efforts either have resulted in much less compliant systems or have required more complicated control systems when compared to prevailing pneumatic ones. The use of rubbery materials leads to this paradox, specifically their easiness of being deformed upon load but, unfortunately, has resisted alteration in the aforementioned effort in load bearing and carrying, probably due to a preconceived notion that soft means rubbery. Is it necessarily true or just a misconception? Can nonrubbery materials be used for pneumatic-driven soft robots and yet simultaneously achieve high compliance and high load-carrying capability to achieve the promise of advanced human robot interactions for complex environments?

Fabrics have been widely adopted in pneumatic actuator designs; however, most as external braids of elastic bladders (*43*, *44*) or strain-limiting layers inside rubbery actuators (*45*, *46*), rendering the mechanical properties of the actuators mainly depending on the rubbery bases. Although other nonrubbery materials (e.g., polyethylene films) can also perform high compliance (*47*, *48*), the weaving technology makes the fabric have better tensile strength and abrasion resistance. Unlike various molding methods for silicone rubbers, the lack of simple, molding-based, readily programmable, and modeling prototyping method makes it challenging to construct complex pneumatic channels inside fabric-based chambers, thus strongly limiting the development of pneumatic actuators made of entire fabric. Most existing designs adopt superpositions of multiple pouches to achieve extension or bending motions (*49*–*51*) or construct cylindrical chambers for structural support (*51*, *52*), due to the low stretchability of the fabric upon inflation. Nevertheless, the bulky structure of multiple pouches results in complicated fabrication and lower compliance, leading to limited workspaces as well as single-mode and less programmable actuation.

Here, we suggest a new design for pneumatic-driven soft robots using unibody fabrics to simultaneously achieve high compliance, high load carrying, and a large workspace (Fig. 1A). Similar to rubbery materials, fabric is soft and human-friendly; yet differently, fabric is not as stretchable as rubbery materials and therefore can bear heavier loads. To obtain a pneumatic actuator with high load-carrying capability while remaining soft, a novel hydrosoluble

[1]State Key Laboratory of Mechanical Systems and Vibration, and Shanghai Key Laboratory of Digital Manufacturing for Thin-Walled Structures, Shanghai Jiao Tong University, Shanghai, 200240, China. [2]School of Engineering, Westlake University, Hangzhou, Zhejiang 310030, China. [3]Meta Robotics Institute, Shanghai Jiao Tong University, Shanghai 200240, China. [4]Research Center for Industries of the Future, Westlake University, Hangzhou, Zhejiang 310030, China.
*Corresponding author. Email: leungchan@sjtu.edu.cn (G.C.); hanqing.jiang@westlake.edu.cn (H.J.)
†These authors contributed equally to this work.

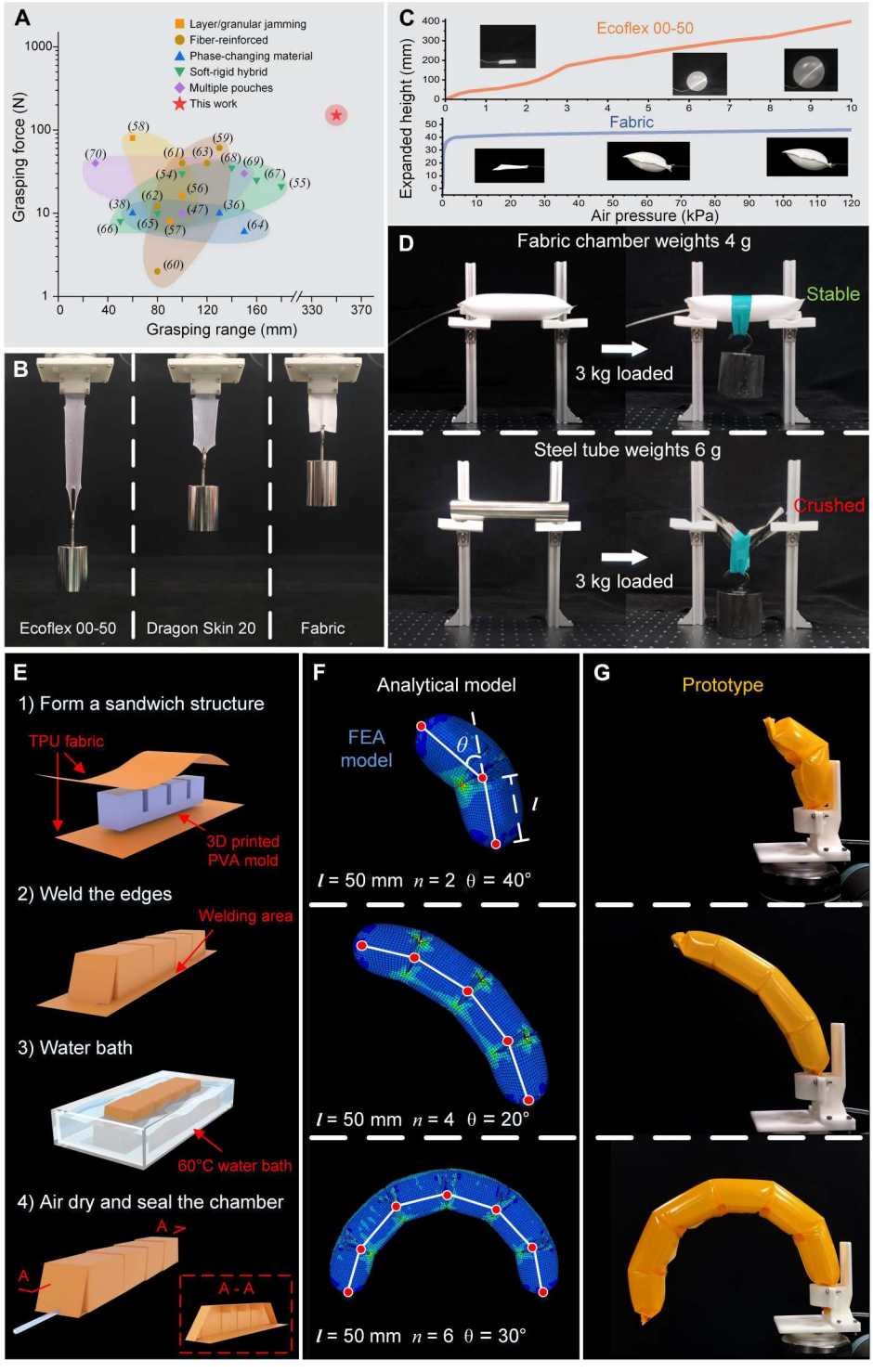

Fig. 1. Construction of the soft pneumatic actuators using soft, lightweight fabrics. (**A**) Comparison of the proposed fabric actuator-based gripper's grasping range and force with various previously developed soft grippers, including the ones with jamming parts (*56*–*58*), ones reinforced by fiber (*59*–*63*), ones integrated with phase-changing materials (*36*, *38*, *64*), ones with soft-rigid hybrid structures (*54*, *55*, *65*–*68*), and ones consisting of multiple pouches (*47*, *69*, *70*). (**B**) Responses of different soft pieces to the same tensile load. The passive stretching of the fabric piece is negligible compared with those of silicone rubber pieces. (**C**) Expanded height versus input pressure of a silicone-based airbag and a fabric-based one. As the pressure increases, the fabric-based airbag rapidly reaches its saturation point without future obvious height increase, while the silicone-based one continues to expand until the explosion. (**D**) Bending comparison between a fabric pneumatic cylinder and a steel tube with similar mass and identical size. The steel tube is readily crushed by a 3-kg weight, while the fabric chamber keeps stable upon the same payload under 45-kPa pressure. (**E**) Fabrication process of the fabric actuator. Step 1: Two pieces of thermoplastic polyurethane (TPU)–coated fabric are tightly attached to the 3D printed polyvinyl alcohol (PVA) mold. Step 2: Weld the overlapped fabric edges with an electric soldering iron. Step 3: Dissolve the internal PVA mold in 60°C water. Step 4: Air dry and seal the chamber together with a pneumatic pipe. The internal structure is shown in the bottom right corner. (**F**) Simulated deformation statuses of different actuators with various body lengths and rotation angles. These deformations can be predicted through both the finite element analysis (FEA) and a theoretical model based on robot kinematics. (**G**) Actual deformation statuses of three actuators with geometric parameters same as the simulated ones.

mold method was developed to make the air channels embedded inside the fabric. The proposed fabric-based pneumatic-driven soft robot has the following merits: lightweight, basically a thin fabric piece and ready for winding when depressurized, easily inflated and unwound to a much larger structure to carry heavy loads when pressurized, and thus simultaneously achieves high compliance and high load-carrying capability. These merits are rooted to the properties of the fabrics, namely, lightweight, highly foldable, yet not that stretchable. By making different air channels inside the fabrics, various deformation modes are demonstrated. This new type of fabric-based pneumatic-driven robots enriches the field of soft robots while paving the way to develop more diversified human-friendly working robots.

RESULTS

Design, fabrication, and actuation principles

The rationale for introducing fabrics for pneumatic-driven soft robots is based on their uniquely different mechanical response upon stretching when compared with rubbery materials. The behavior of fabric versus rubber can be characterized via the uniaxial tension test (Fig. 1B). Upon quantitative uniaxial tension, two rubbery materials (Ecoflex 00-50 and Dragon Skin 20 with thickness of 1.5 mm and mass of 1.02 and 1.40 g) exhibited 18- and 15-fold higher stretchability than a 0.25-mm-thick and 0.13-g piece of fabric, showing a 680.68% breaking strain for Ecoflex and 564.12% for Dragon Skin. This stands in contrast to the 37.76% for fabrics, which, in turn, is due to the much lower moduli of the rubbery materials when compared with the fabrics. As shown in fig. S1, the two rubbery materials have more than 1000 and 300 times lower modulus than that of the fabrics (i.e., 0.10 MPa for Ecoflex and 0.41 MPa for Dragon Skin versus 127.81 MPa for fabrics). As shown in Fig. 1C, the airbag made of thermoplastic polyurethane (TPU)–coated fabric bears higher pressure and does not exhibit continuous expansion compared to the rubbery one. This fabric-based airbag is seen to reach a saturated state after inflating at low pressure; moreover, when a continuous increase in pressure is applied to the fabric airbag, it contributes to the structural stiffness of the fabric rather than its structural deformation, in contrast to the rubbery material. Eventually, the critical point of pressure for explosion for the fabric airbag increases 12-fold as opposed to the rubbery airbag, which holds at 120 kPa for the TPU-coated fabric airbag with a thickness of 0.3 mm and 5.5 g in mass versus 10 kPa for the rubbery airbag with a thickness of 2 mm and 29.5 g in mass. Thus, from saturation point to explosion point, the pressure inside the airbag increases 40-fold, while the height of the airbag just increases 11%, thereby establishing its potential for load-carrying capability. Its counterpart made up of rubbery materials, on the other hand, shows a continuous increase in both pressure and volumetric deformation, indicating a low load-carrying capability.

When a fabric chamber with 200 mm in length and 30 mm in diameter (with mass of 4 g) is pressurized under 45-kPa pressure, its bending rigidity is capable of carrying a 3-kg weight without obvious deflection (Fig. 1D). As a fair comparison, a steel tube under the constraints of similar mass (i.e., 6 g) and size (i.e., 200 mm in length and 30 mm in diameter) can be seen as not being able to carry the same 3-kg payload. It should be noted, however, that, so far, the deformation is isotropic upon pressure, whereas the features of the fabric air chambers are now needed for nonsymmetric (e.g., bending and twisting) deformation modes.

A readily replicable, molding-based fabrication method for TPU-coated fabric was developed to define the features of the air chambers for nonsymmetric deformation upon pressure (Fig. 1E). The inner mold made up of a three-dimensional (3D) printed hydrosoluble material [e.g., polyvinyl alcohol (PVA)] was wrapped with two pieces of fabrics to form a sandwiched structure, whose edges were heat-sealed and clipped, leaving a small opening for the next step. The sandwich structure was then immersed in a 60°C water bath for 4 hours to remove the hydrosoluble material, followed by sealing of the small opening. This process results in the creation of a hollow, fabric-based air chamber (see Materials and Methods for details). As suggested by Fig. 1C, small inflation after the saturation point makes the formed fabric chamber have a nearly fixed deformation mode upon pressure, rendering the nonsymmetric deformation motion more powerful and predictable. A direct comparison between a fabric-based chamber and a silicone-based one with similar geometric parameters under the same input pressure is demonstrated in table S1, showing that the fabric-based design exhibits a higher output force with a substantial decrease in dead weight.

The deformation of the proposed fabric chamber depends on three variables: rotation angle θ, the number of the segments n, and the length of the segments l (Fig. 1F), which can be derived from the geometric parameters of the inner mold (see text S1 and fig. S2 for details). Here, we keep the length of the segments constant while controlling both for angle θ and number of segments n. We then apply finite element analysis (FEA) for the pressurized fabric chamber (see Materials and Methods for details) and develop an analytical kinematic model based on the robot kinematics theories (text S1, fig. S3, and table S2) for predicting the deformation status of the designed chambers with different parameters. Figure 1 (F and G) demonstrates the simulated (both FEA and analytical model) and experimental results of three chambers with different design parameters, all in good agreement (more comparisons shown in figs. S4 to S6). Thus, these experiments show that the motion of a specific chamber can be predicted using the proposed model while simultaneously offering the ability to customize through appropriate parameter adjustments.

Mechanical properties of the fabric-based air chambers

The mechanical properties of the fabric-based air chambers were characterized in terms of response time, generated force, and stiffness (Fig. 2). The parameters of the PVA mold to construct the air chambers are provided in fig. S2, and only chambers with straight grooves are considered here. The effects of the groove angles will be discussed in the next section. Figure 2A shows that a fabric-based air chamber of 250 mm in length and 25 mm in radius can reach its fully expanded and bent state in approximately 600 ms. This rapid response is due to the fact that the input pressure mainly inflates the fabric chamber rather than stretching the material to generate elastic deformation, as opposed to the situation for the rubbery ones. The actuation speed is mainly restricted by the flow rate of the compressed air and can be further enhanced by shortening the effective length of the chamber (Fig. 2B). In addition to response time, the present fabric-based actuator also exhibits enhanced output force, also due to the slight deformation of the fabric air chambers upon pressure. The blocked force at the tip of the actuator at varying pressures of the three chambers with different lengths was also measured (Fig. 2C and fig. S8). It was found that, for an air chamber with 200 mm in length and 25 mm in radius, the generated force can be up to 45 N at 50 kPa, representing a significant enhancement compared to conventional designs based on silicone rubber (*53*–*55*). The output force also showed a tendency to increase, with increases in rotation angle θ [= $\arctan(2h_i/H)$; see fig. S2 for details] and actuator length L (= nl) (Fig. 2, C and D).

Similar to the air chambers without any grooves (i.e., simple expansion as shown in Fig. 1D), air chambers with grooves are able to hold the morphing status under payload. As shown in Fig. 2E, under a 1-kg weight, there is very small deflection for a 12-g chamber under 50-kPa pressure, and a slightly larger deflection under smaller pressure (i.e., 10 kPa). We further conducted stiffness tests with three chambers of different lengths (Fig. 2, F to H, and

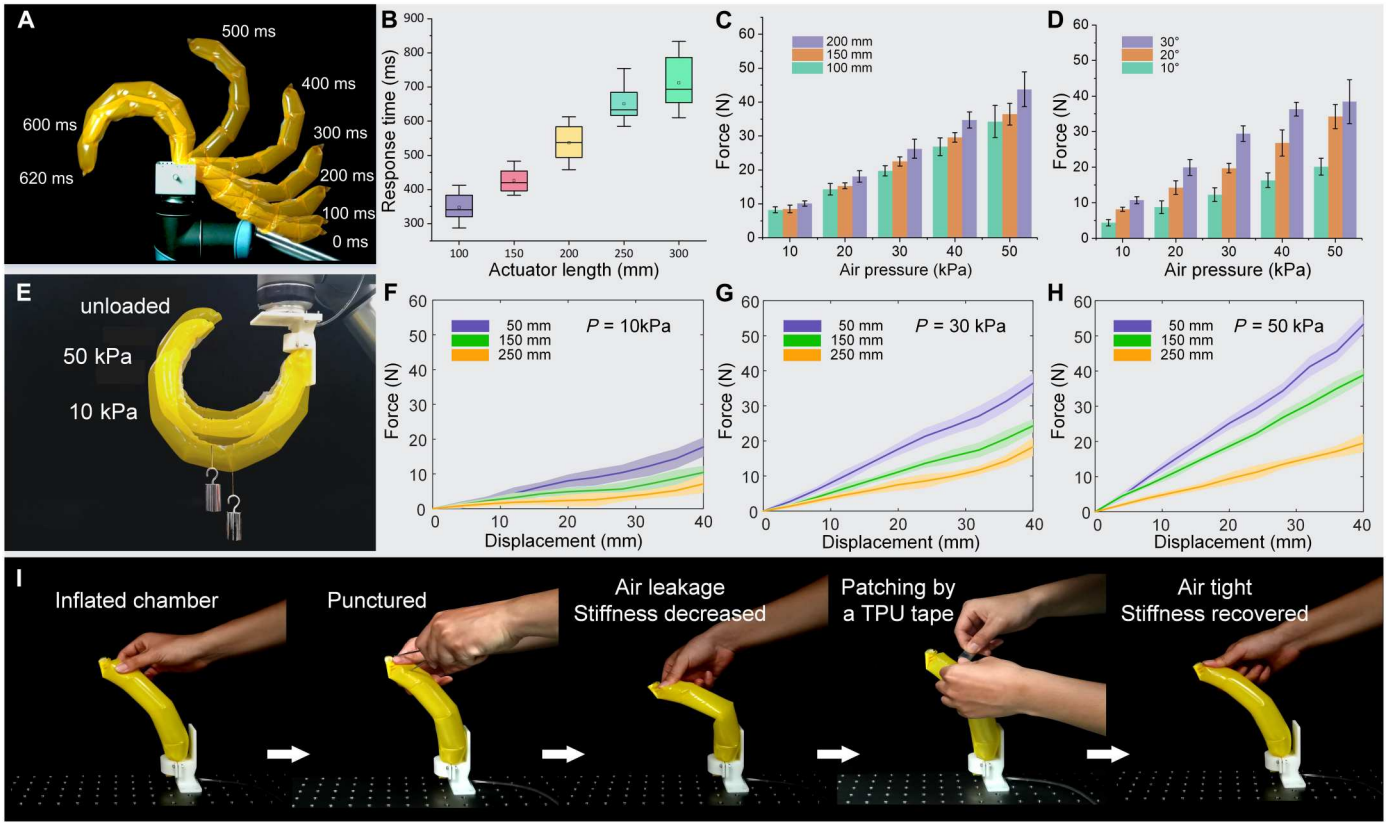

Fig. 2. Mechanical properties of the fabric actuator. (**A**) Response of a 250-mm-long actuator upon inflation. (**B**) Required times for reaching deformation limits. Five actuators with body lengths between 100 and 300 mm were tested. (**C**) Tip blocked force of three actuators in different body lengths at different pressure values. (**D**) Tip blocked force of three actuators with different rotation angles at different pressure values. (**E**) Comparison of an unloaded bending actuator and a 1-kg loaded actuator with input pressure of 10 and 50 kPa. (**F** to **H**) Stiffness curves of actuators in different body lengths at different pressures. Actuator stiffness showed positive correlation with pressure and negative correlation with body length. (**I**) Simple, quick repair process of a leaked/damaged actuator. The patched actuator can almost restore to its original performance.

figs. S8 and S9). From these tests, it is apparent that the chamber with higher input pressure required a higher force to deform, while the stiffness of the nonsymmetric air chambers depended on the geometries, which is in accordance with the proposed mechanical model (text S2 and figs. S10 to S13). This analytical mechanical model, together with the kinematic model proposed in the above section, can guide the customization of the fabric air chamber according to the required workspace and stiffness. In addition, the present fabric chamber has high robustness upon pressure, exhibiting a constant output force under a specific input pressure after 1000 times of inflation and deflation (fig. S14). Another exciting feature of the fabric chamber is its repairability. After being punctured by piercing objects (tender spots for most fluidic actuators), the hole in the chamber can be readily patched using a TPU tape (Fig. 2I); moreover, the stiffness of the chamber can also be recovered due to the reobtained air tightness.

Programmable and combinable actuation mode

The groove angles of the actuator play a pivotal role in controlling the deformation mode, which can also be readily programmed by adjusting the groove angle of the hydrosoluble mold. Figure 3A demonstrates three actuators with identical lengths (300 mm) and radii (15 mm), but with different groove angles. Specifically, air chambers with no grooves lead to a straightening deformation mode (i.e., no bending and twisting), straight grooves (groove angle $\phi = 0$) lead to bending deformation, and inclined grooves (groove angle $\phi > 0$) cause twisting deformation. Furthermore, owing to the convenience from the welding-based fabrication with the thin fabric, more complex motions can be exhibited on a single actuator. As shown in Fig. 3B, the mold can be divided into two or three parts in axial direction, defining different grooves. The three basic actuation modes (i.e., straightening, bending, and twisting) in Fig. 3A then successionally appear on one slender chamber once pressurized. Note that more complex motion types can be readily achieved by arranging different grooves on the same mold as needed.

In addition to being serially connected, the various actuation modes can be combined in a parallel manner with each one being individually controllable. Figure 3C illustrates the fabrication steps and the experimental results, in which the mold for the first chamber has no grooves, and thus, the actuator straightens when its pressure P_1 is activated, the second chamber uses a mold with straight grooves and leads to a bending mode upon P_2, and the third chamber uses a mold with inclined grooves and twists upon P_3. Unlike conventional silicone-based pneumatic actuators with hard-to-compress, thick structures, the fabric chambers can be

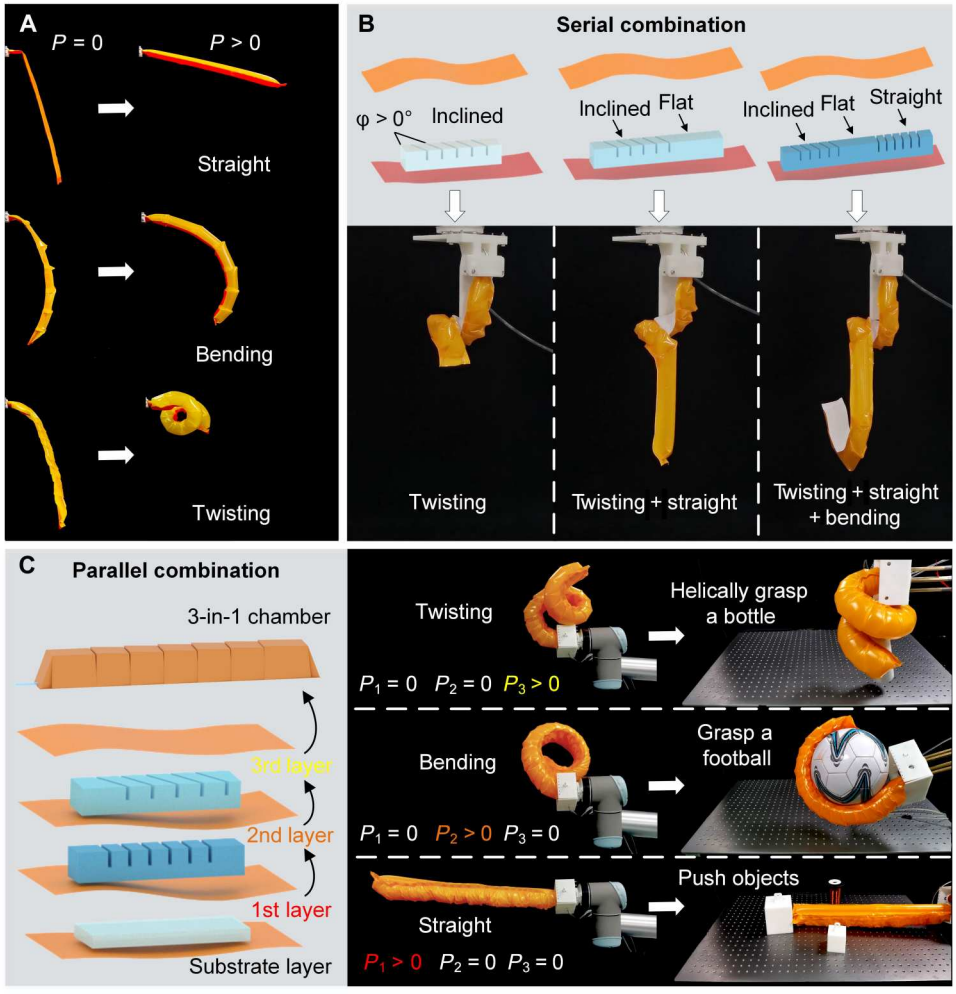

Fig. 3. Programmable actuation modes and their combinations in a single actuator. (**A**) Three basic actuation modes of the actuator: straightening, bending, and twisting. (**B**) Fabrication method and outcomes of serial combination. Segmented, complex motions can be achieved on a single slender actuator. (**C**) Fabrication method and outcomes of parallel combination. The top chamber is fabricated after the mold inside the bottom chamber is dissolved. A single prototype can then exhibit various motion modes and freely switch among these modes according to different scenarios.

readily compressed into a flat sheet, making it possible to laminate multiple chambers with different motion modes layer by layer. In this way, rapid reconfiguration can be achieved through one actuator by selecting different chambers to inflate, which, in conventional actuators, typically requires radially spacing multiple actuators or manual assistance (*22*–*24*). Multi-df dexterous motion and reconfiguration have long been highly desirable features for soft robots. Our solution exploits the advantages of fabric pieces while proposing a versatile, lightweight actuator with simple construction. As depicted in Fig. 3C, a single actuator can perform various motion types according to different scenarios, benefiting from its combined actuation modes.

Windable structure and tunable effective length

As introduced in previous sections, the bending angle θ, groove angle ϕ, and body length L are design parameters that determine the shape morphing of the proposed actuator. Among these parameters, the first two are preset and nonadjustable after fabrication; however, the effective body length is potentially adjustable. Unlike silicone-based pneumatic actuators with hard-to-compress bodies, the present unibody fabric chambers are soft and compressible, making a deflated chamber readily compressed into a flat sheet and windable around a roller. Hence, a winding mechanism was designed to expand the workspace of the actuator through automatically controlling its effective length. As shown in Fig. 4A, the proximal end of a fabric chamber is attached to a motor-controlled cylindrical roller. A second roller that rotates in the opposite direction of the actuated one through gear transmission is used to compress the wound chamber and to ensure the regularity of the winding and releasing process.

Figure 4B demonstrates the actuation process of a fabric chamber with variable effective lengths. Benefiting from its compressible feature, the fabric chamber can be wholly wound inside the base when deflated, making the whole system readily packable. Upon the roller's rotation, the chamber can be released from the base, thereby exhibiting different bending modes upon inflation at different lengths. Moreover, the fabric chamber can be rewound on the roller again after deflation, rendering it capable

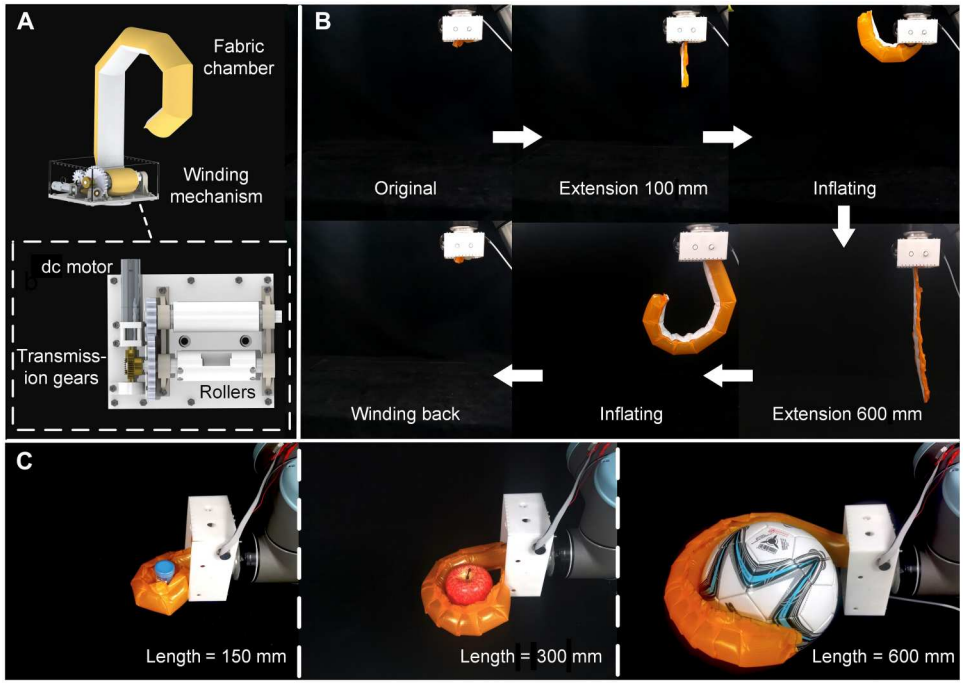

Fig. 4. Windable structure results in tunable actuator length. (**A**) Schematics of the fabric actuator with tunable length. A winding mechanism is designed to control the effective length of the actuator. (**B**) Actuation process of a fabric chamber with variable effective lengths. A 600-mm actuator can be fully wound inside a small base box and inflated at any length. (**C**) Tuning the effective length to better conform to different target objects. The selected objects have diameters from 60 to 220 mm.

of freely adjusting for suitable length according to various interacted objects. Note that the bending status at any effective length is relative to the design parameters, which can be predicted on the basis of the theoretical model introduced before. To further demonstrate the significance of the tunable length, we used an actuator prototype to grasp three objects with different diameters ranging from 60 to 220 mm. Images from our experiments in Fig. 4C show that the actuator exhibits stable grasping at various lengths. The tunable length renders it better able to conform to different target objects.

Powerful soft gripper with large grasping range

A three-fingered robotic gripper is designed to further exploit our actuator′s merits in load-carrying and tunable body length. Here, each finger is a parallel combination of a bending chamber and a straight one. A rapid switch between pick and place manipulation can then be readily achieved by switching the inflated/deflated chamber. As to the winding mechanism, three rollers are used to make the length of each finger independently adjustable, leading to more various grasping modes (additional details of the mechanical design shown in fig. S15). Figure 5 (A to D) illustrates the mechanical design, the variable finger length, and the quantified grasping capability of a gripper prototype. The pull-off force under three different finger lengths ranging from 150 to 250 mm was tested. The maximum grasping force under 150 mm exceeds 150 N, more than 400 times the dead weight of each finger. The grasping force slightly decreases with increase in finger length, which is reasonable due to the increased bending moment. The high performance in both grasping range and grasping force makes our gripper a unique design among existing soft grippers, which typically exhibit low payload and limited workspace (Fig. 1A, with more detailed parameters in table S3). Owing to the windable fingers, the grasping range of our gripper is significantly improved compared with conventional ones with fixed finger lengths (*36*, *38*, *47*, *54*–*70*). As well, the less stretchable fabric structure, together with the input pressure, renders the soft gripper insensitive to a high payload, making it one of the most powerful designs.

To better frame the gripper′s practical performance, we performed a series of grasping tests with some typical objects from the Yale-Columbia-Berkeley object set (*71*), as well as several large-scale heavy objects commonly used in our daily life (table S4 and fig. S16). Figure 5E demonstrates one of the grasping processes, under an actuation pressure of less than 50 kPa. By actively tuning the effective finger length, the gripper can grasp small, light objects (e.g., a tennis ball) or large, heavy objects (e.g., a storage box with items or even a big teddy bear together with the bar stool it sits on) (Fig. 5F). The lightest object is less than 50 g with a diameter of less than 70 mm; the heaviest object, namely, the bar stool with dumbbell pieces, is more than 7 kg with a diameter of more than 350 mm and of a much larger length. In addition, a two-fingered gripper with a more compact structure is also applicable based on the proposed design strategy. More details about the grasping process are presented in movie S9 and figs. S17 and S18. Note that the highest payload of our gripper is close to the load limit of the connected industrial robot (UR10, Universal Robots Inc.), making it a low-cost, easy-to-fabricate, soft gripper with sufficient strength for robotic applications.

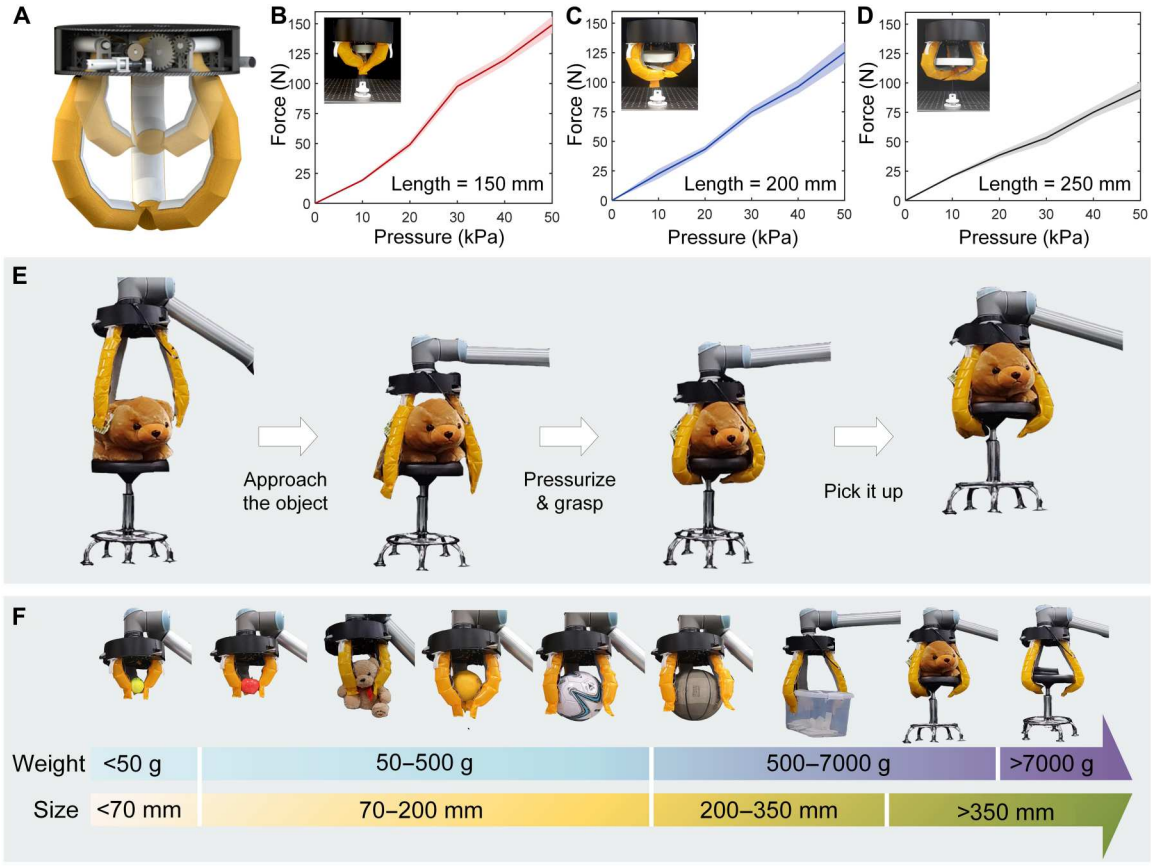

Fig. 5. Powerful soft robotic gripper with variable grasping range. (**A**) Schematics of the gripper. (**B** to **D**) Pull-off force of the gripper at different finger lengths. (**E**) Grasping and lifting a stool with a big teddy bear. (**F**) Tested objects. The diameters of the objects are from 70 to 350 mm, and their weights are from 50 to 7050 g.

DISCUSSION

In summary, this paper reports a new methodology for the design, fabrication, and analysis of fabric-based soft pneumatic actuators having high-range and powerful actuation. The low stretchability of the used fabric renders the actuator readily inflatable, more pressure resistant, and less sensitive to external loads than existing actuators. The high-range motion of the actuator is realized by controlling its effective body length through winding and by benefitting from the soft, hollow, and easily compressible structure of the fabric chamber. Accordingly, the robotic gripper, consisting of three fabric actuators, is demonstrated to show a powerful grasping capability with a maximum grasping force of over 150 N and a grasping range of over 350 mm, thereby making it one of the most powerful and adaptable designs among the existing soft grippers. Through designing the geometric parameters of the hydrosoluble 3D printed mold and deformation analysis based on the proposed models, this work enables the pressurized actuator to be both programmable and combinable, thus enriching its motion versatility and overall functionality. Other merits of the developed fabric actuator include its simple fabrication method, fast response time, easy maintenance, and low cost. Introducing this type of fabric for building soft robots opens possibilities for attracting more advanced fiber technologies into robotic applications (*72*–*74*). The proposed actuator carries high potential to be integrated with other functions, such as tactile sensing, 3D displays, and wearable haptics.

MATERIALS AND METHODS

Fabrication details

We have proposed here a reverse-molding method to form customized, irregular pneumatic chambers based on weaved fabric. First, we wrap two pieces of TPU-coated fabric (TPU-N20D, Jiaxing Inch Eco-Materials Inc.) around a 3D printed PVA mold. The proposed mold can be customized according to different requirements of various motion modes. It can also be printed using a commercial fused deposition modeling 3D printer (E2, Raise 3D Inc.), with printing parameters shown in table S5. The overlapped edges of the two pieces were welded using an electric soldering iron with a temperature of 220°C. During this process, we reserved a 20-mm unwelded area on the short side to ensure that the water soaked the wrapped PVA mold. The dissolution of the mold can be completed in 4 hours in a 60°C water bath. A silicone air tube (2 mm inner diameter) was then connected to the chamber by an ethylene-vinyl acetate copolymer hot-melt adhesive. After the chamber was fully formed, cleaned, and dried, the welded surfaces were trimmed with scissors to make the whole structure neater. As for the fingers of the length-tunable gripper, additional pieces of cotton-polyester

fabric were welded on the inner sides of the fingers to add friction between the gripper and objects.

FEA of the fabric chamber

CAD modeling

We constructed the computer aided design (CAD) model of the pneumatic chambers with a commercial software (Solidworks 2019, Dassault Systemes Inc.). First, we created a cuboid structure with the same external dimensions as the real pneumatic chamber. Both ends of the cuboid were cut into similar external shapes as the real chamber. To reconstruct the joints and folding valleys in the chamber, we used an extruded cut to simulate the creases on a TPU-coated fabric. The size and position of the cuts were made the same as the designed parameter of the pneumatic chamber. During the modeling process, the width of each cut was limited to 0.5 mm to simulate the creases in a real chamber. After the joints and folding valleys were constructed, the inner part of the model was deleted to create the hollow air chamber (fig. S19). Because surface pressure was used to simulate the inflation process of the chamber during the FEA simulation process, the air tube in the real prototype was omitted in the CAD model.

Finite element analysis

The CAD model of the pneumatic chambers was imported into an FEA software (ABAQUS, Dassault Systemes Inc.) to perform the simulation. We discretized the models using a mesh of four-sided linear shell elements (ABAQUS element type, S4R), with a mesh size adapted to ensure that at least nine elements are used to discretize each surface of the chamber. To simulate the material properties of the TPU-coated fabric, we used the keyword *Fabric in ABAQUS to define the in-plane behavior. The density of the material was set at 780 kg/m^3, according to the property of real TPU-coated fabric. The material properties of TPU-coated fabric were defined with a nonlinear elastic model, with the elastic modulus of 120 MPa and the Poisson′s ratio of 0.49. We specified the uniaxial behavior of the material in the warp and weft directions, as well as the shear behavior. To remove the rigid body translation and rotation of the pneumatic chamber, we imposed a full constraint boundary condition ($u_x = u_y = u_z = u_{Rx} = u_{Ry} = u_{Rz} = 0$) at the one end of the chamber. The inflation of the models was controlled by a static pressure imposed on the inner surface of the air chamber, which was set at 30 kPa for each model. For each of the simulation models that we created according to the ones in the experiment, a side view was recorded after being fully inflated. The rotation axes were located at each joint between the chambers. The angle formed by the mesh on both sides of the rotation center indicated the rotation angle (fig. S19). The rotation angles in all three simulations were identical, in accordance with the experimental results.

Pneumatic control

The pneumatic control system can be divided into three parts, each responsible for air supply, pressure control, and pressure feedback (fig. S20). The internal pressure of the fabric actuator was provided by an air pump and regulated by a PSOL (Proportional Solenoid, ITV1010, SMC Inc.) powered by a regulated 24-V supply. The signal from the microcontroller (Mega 2560, Arduino Inc.) was processed by a digital to analog convertor (DAC) module (DC2376A-A, ADI Inc.), which was powered by a regulated 12-V supply and sent to the PSOL. The actuation pressure was collected in real time by a pressure sensor (PSE532, SMC Inc.) through a serial protocol interface; it then formed the feedback control of the pneumatic pressure. Here, PID (proportional, integral, and differential) control was used to realize a rapid response to the given pressure. Such a closed-loop system could also keep the inner pressure of the actuator around the prescribed value during the motion. It should be noted that the number of PSOL and pressure sensors was increased by a factor of 3 for the parallel actuator with three different motion modes. Each inner chamber was actuated with different independent PID parameters, due to the different volumes of the chambers.

Actuator length control

To precisely control the effective length of the actuator, a high-quality dc motor (DCX16, Maxon Inc.) was used to control the winding of the fabric chamber through the 3D printed cylindrical roller. The control signal was sent by the personal computer (PC), first passed through the controller (AX5000, BECKHOFF Inc.) and then drove the motor to rotate through a motor drive (fig. S21). As to the three-fingered gripper, the numbers of the motor and the corresponding transmission parts were increased by a factor of 3, making the length of each gripper independently tunable. Worm gears are included between each roller and dc motor. Besides amplifying the output torque, the worm gears provide self-locking capability, avoiding the motors being affected by the payload and then ensuring the selected actuator length.

Characterization of the fabric pneumatic actuator

Deformation characterization

To measure the response of the actuator, we recorded the motion trial with a high-speed camera (PrimeColor, OptiTrack Inc.). The initial pressure of the actuator in each experiment is the same as the external atmosphere. The motion of the actuator is recorded after pressurization. Similarly, to characterize the deformation of the actuators with different effective lengths and variable rotation angles, we analyzed the real-time deformations through images. The side view of each actuator was taken using a commercial camera (EOS 700D, Canon Inc.). The rotation axes are located at the intersections of the chamber′s welding edges and folding valleys. The angle formed by the fabric linkages on both sides of the rotation axis denotes the rotation angle.

Output force characterization

To characterize the output force of the fabric actuator with different effective lengths under different input pressure, we measured the actuator′s relationship between the tip blocked force and the air pressure (fig. S8A). The force was measured using a force sensor (Mini45, ATI Inc.) fixed upon the end-effector of a six-df industrial robot (UR10, Universal Robots Inc.). The effective length of the tested actuator ranged from 100 to 200 mm, with an increment of 50 mm. The input pressure in each test was from 10 to 50 kPa. The industrial robot remained stationary during each test.

Stiffness characterization

To characterize the stiffness of our actuator with different effective lengths under different input pressure, we measured the actuator′s relationship between the passive displacement and the generated force. This setup is similar to that of output force tests, with the only difference being that the industrial robot actively pulls the actuators (fig. S8B). The effective lengths of the tested actuators ranged from 50 to 250 mm, with an increment of 50 mm. The input pressure was set from 10 to 50 kPa.

Robustness characterization

To characterize the robustness of our actuator, we measured the actuator's output force and input pressure value upon 1000 times of inflation and deflation. The experimental setup is similar to that of the stiffness tests shown in fig. S8B. A bending actuator is vertically fixed on a platform, with its distal end connected with a fixed force sensor through a KEVLAR rope. The industrial robot remained stationary, while the input pressure was set as 40 kPa and periodically inflated the chamber through an actively controlled solenoid valve at a frequency of 1 Hz.

Supplementary Materials

This PDF file includes:

Supplementary Text
Figs. S1 to S21
Tables S1 to S5
Legends for movies S1 to S9
References

Other Supplementary Material for this manuscript includes the following:

Movies S1 to S9

REFERENCES AND NOTES

1. R. F. Shepherd, F. Ilievski, W. Choi, S. A. Morin, A. A. Stokes, A. D. Mazzeo, X. Chen, M. Wang, G. M. Whitesides, Multigait soft robot. *Proc. Natl. Acad. Sci. U.S.A.* **108**, 20400–20403 (2011).
2. S. W. Kwok, S. A. Morin, B. Mosadegh, J. H. So, R. F. Shepherd, R. V. Martinez, B. Smith, F. C. Simeone, A. A. Stokes, G. M. Whitesides, Magnetic assembly of soft robots with hard components. *Adv. Funct. Mater.* **24**, 2180–2187 (2014).
3. R. K. Katzschmann, J. DelPreto, R. MacCurdy, D. Rus, Exploration of underwater life with an acoustically controlled soft robotic fish. *Sci. Robot.* **3**, eaar3449 (2018).
4. Y. Tang, Y. Chi, J. Sun, T.-H. Huang, O. H. Maghsoudi, A. Spence, J. Zhao, H. Su, J. Yin, Leveraging elastic instabilities for amplified performance: Spine-inspired high-speed and high-force soft robots. *Sci. Adv.* **6**, eaaz6912 (2020).
5. G. Mao, M. Drack, M. Karami-Mosammam, D. Wirthl, T. Stockinger, R. Schwodiauer, M. Kaltenbrunner, Soft electromagnetic actuators. *Sci. Adv.* **6**, eabc0251 (2020).
6. R. V. Martinez, J. L. Branch, C. R. Fish, L. Jin, R. F. Shepherd, R. M. Nunes, Z. Suo, G. M. Whitesides, Robotic tentacles with three-dimensional mobility based on flexible elastomers. *Adv. Mater.* **25**, 205–212 (2013).
7. M. Schaffner, J. A. Faber, L. Pianegonda, P. A. Rühs, F. Coulter, A. R. Studart, 3D printing of robotic soft actuators with programmable bioinspired architectures. *Nat. Commun.* **9**, 878 (2018).
8. R. A. Shveda, A. Rajappan, T. F. Yap, Z. Liu, M. D. Bell, B. Jumet, V. Sanchez, D. J. Preston, A wearable textile-based pneumatic energy harvesting system for assistive robotics. *Sci. Adv.* **8**, eabo2418 (2022).
9. Q. Ze, S. Wu, J. Dai, S. Leanza, G. Ikeda, P. C. Yang, G. Iaccarino, R. R. Zhao, Spinning-enabled wireless amphibious origami millirobot. *Nat. Commun.* **13**, 3118 (2022).
10. Y. S. Choi, H. Jeong, R. T. Yin, R. Avila, A. Pfenniger, J. Yoo, J. Y. Lee, A. Tzavelis, Y. J. Lee, S. W. Chen, H. S. Knight, S. Kim, H.-Y. Ahn, G. Wickerson, A. Vázquez-Guardado, E. Higbee-Dempsey, B. A. Russo, M. A. Napolitano, T. J. Holleran, L. A. Razzak, A. N. Miniovich, G. Lee, B. Geist, B. Kim, S. Han, J. A. Brennan, K. Aras, S. S. Kwak, J. Kim, E. A. Waters, X. Yang, A. Burrell, K. San Chun, C. Liu, C. Wu, A. Y. Rwei, A. N. Spann, A. Banks, D. Johnson, Z. J. Zhang, C. R. Haney, S. H. Jin, A. V. Sahakian, Y. Huang, G. D. Trachiotis, B. P. Knight, R. K. Arora, I. R. Efimov, J. A. Rogers, A transient, closed-loop network of wireless, body-integrated devices for autonomous electrotherapy. *Science* **376**, 1006–1012 (2022).
11. D. Rus, M. T. Tolley, Design, fabrication and control of soft robots. *Nature* **521**, 467–475 (2015).
12. H. Zhao, A. M. Hussain, M. Duduta, D. M. Vogt, R. J. Wood, D. R. Clarke, Compact dielectric elastomer linear actuators. *Adv. Funct. Mater.* **28**, 1804328 (2018).
13. R. Chen, Z. Yuan, J. Guo, L. Bai, X. Zhu, F. Liu, H. Pu, L. Xin, Y. Peng, J. Luo, L. Wen, Y. Sun, Legless soft robots capable of rapid, continuous, and steered jumping. *Nat. Commun.* **12**, 1–12 (2021).
14. C. Laschi, M. Cianchetti, B. Mazzolai, L. Margheri, M. Follador, P. Dario, Soft robot arm inspired by the octopus. *Adv. Robot.* **26**, 709–727 (2012).
15. Z. Zhakypov, K. Mori, K. Hosoda, J. Paik, Designing minimal and scalable insect-inspired multi-locomotion millirobots. *Nature* **571**, 381–386 (2019).
16. Z. Hu, Y. Li, J.-a. Lv, Phototunable self-oscillating system driven by a self-winding fiber actuator. *Nat. Commun.* **12**, 3211 (2021).
17. S. Li, H. Bai, Z. Liu, X. Zhang, C. Huang, L. W. Wiesner, M. Silberstein, R. F. Shepherd, Digital light processing of liquid crystal elastomers for self-sensing artificial muscles. *Sci. Adv.* **7**, eabg3677 (2021).
18. S. Wu, Q. Ze, J. Dai, N. Udipi, G. H. Paulino, R. Zhao, Stretchable origami robotic arm with omnidirectional bending and twisting. *Proc. Natl. Acad. Sci.* **118**, e2110023118 (2021).
19. Q. Ze, S. Wu, J. Nishikawa, J. Dai, Y. Sun, S. Leanza, C. Zemelka, L. S. Novelino, G. H. Paulino, R. R. Zhao, Soft robotic origami crawler. *Sci. Adv.* **8**, eabm7834 (2022).
20. B. Gorissen, D. Reynaerts, S. Konishi, K. Yoshida, J. W. Kim, M. De Volder, Elastic inflatable actuators for soft robotic applications. *Adv. Mater.* **29**, 1604977 (2017).
21. R. V. Martinez, C. R. Fish, X. Chen, G. M. Whitesides, Elastomeric origami: Programmable paper-elastomer composites as pneumatic actuators. *Adv. Funct. Mater.* **22**, 1376–1384 (2012).
22. S. Y. Kim, R. Baines, J. Booth, N. Vasios, K. Bertoldi, R. Kramer-Bottiglio, Reconfigurable soft body trajectories using unidirectionally stretchable composite laminae. *Nat. Commun.* **10**, 3464 (2019).
23. B. Yang, R. Baines, D. Shah, S. Patiballa, E. Thomas, M. Venkadesan, R. Kramer-Bottiglio, Reprogrammable soft actuation and shape-shifting via tensile jamming. *Sci. Adv.* **7**, eabh2073 (2021).
24. J. Zou, M. Feng, N. Ding, P. Yan, H. Xu, D. Yang, N. X. Fang, G. Gu, X. Zhu, Muscle-fiber array inspired, multiple-mode, pneumatic artificial muscles through planar design and one-step rolling fabrication. *Natl. Sci. Rev.* **8**, nwab048 (2021).
25. L. Paez, G. Agarwal, J. Paik, Design and analysis of a soft pneumatic actuator with origami shell reinforcement. *Soft Robot.* **3**, 109–119 (2016).
26. Y. Chen, F. Wan, T. Wu, C. Song, Soft-rigid interaction mechanism towards a lobster-inspired hybrid actuator. *J. Micromech. Microeng.* **28**, 014007 (2017).
27. J. Zhang, T. Wang, J. Wang, M. Y. Wang, B. Li, J. X. Zhang, J. Hong, Geometric confined pneumatic soft–rigid hybrid actuators. *Soft Robot.* **7**, 574–582 (2020).
28. B. Verrelst, R. V. Ham, B. Vanderborght, F. Daerden, D. Lefeber, J. Vermeulen, The pneumatic biped "Lucy" actuated with pleated pneumatic artificial muscles. *Auton. Robots* **18**, 201–213 (2005).
29. G. Andrikopoulos, G. Nikolakopoulos, S. Manesis, Advanced nonlinear PID-based antagonistic control for pneumatic muscle actuators. *IEEE Trans. Ind. Electron.* **61**, 6926–6937 (2014).
30. Z. Zhang, G. Chen, H. Wu, L. Kong, H. Wang, A pneumatic/cable-driven hybrid linear actuator with combined structure of origami chambers and deployable mechanism. *IEEE Robot. Autom. Lett.* **5**, 3564–3571 (2020).
31. Z. Zhang, S. Tang, W. Fan, Y. Xun, H. Wang, G. Chen, Design and analysis of hybrid-driven origami continuum robots with extensible and stiffness-tunable sections. *Mech. Mach. Theory* **169**, 104607 (2022).
32. E. Brown, N. Rodenberg, J. Amend, A. Mozeika, E. Steltz, M. R. Zakin, H. Lipson, H. M. Jaeger, Universal robotic gripper based on the jamming of granular material. *Proc. Natl. Acad. Sci. U.S.A.* **107**, 18809–18814 (2010).
33. Y. S. Narang, J. J. Vlassak, R. D. Howe, Mechanically versatile soft machines through laminar jamming. *Adv. Funct. Mater.* **28**, 1707136 (2018).
34. Y. Wang, L. Li, D. Hofmann, J. E. Andrade, C. Daraio, Structured fabrics with tunable mechanical properties. *Nature* **596**, 238–243 (2021).
35. W. Shan, T. Lu, C. Majidi, Soft-matter composites with electrically tunable elastic rigidity. *Smart Mater. Struct.* **22**, 085005 (2013).
36. M. Al-Rubaiai, T. Pinto, C. Qian, X. Tan, Soft actuators with stiffness and shape modulation using 3D-printed conductive polylactic acid material. *Soft Robot.* **6**, 318–332 (2019).
37. Y. Yang, Y. Chen, Y. Li, Z. Wang, Y. Li, Novel variable-stiffness robotic fingers with built-in position feedback. *Soft Robot.* **4**, 338–352 (2017).
38. Y. F. Zhang, N. Zhang, H. Hingorani, N. Ding, D. Wang, C. Yuan, B. Zhang, G. Gu, Q. Ge, Fast-response, stiffness-tunable soft actuator by hybrid multimaterial 3D printing. *Adv. Funct. Mater.* **29**, 1806698 (2019).
39. C. Cao, X. Zhao, Tunable stiffness of electrorheological elastomers by designing mesostructures. *Appl. Phys. Lett.* **103**, 041901 (2013).
40. S. B. Behbahani, X. Tan, Design and dynamic modeling of electrorheological fluid-based variable-stiffness fin for robotic fish. *Smart Mater. Struct.* **26**, 085014 (2017).
41. C. Majidi, R. J. Wood, Tunable elastic stiffness with microconfined magnetorheological domains at low magnetic field. *Appl. Phys. Lett.* **97**, 164104 (2010).
42. V. Lara-Prieto, R. Parkin, M. Jackson, V. Silberschmidt, Z. Kęsy, Vibration characteristics of MR cantilever sandwich beams: Experimental study. *Smart Mater. Struct.* **19**, 015005 (2009).

43. S. Davis, D. G. Caldwell, Braid effects on contractile range and friction modeling in pneumatic muscle actuators. *Int. J. Rob. Res.* **25**, 359–369 (2006).
44. L. Cappello, K. C. Galloway, S. Sanan, D. A. Wagner, R. Granberry, S. Engelhardt, F. L. Haufe, J. D. Peisner, C. J. Walsh, Exploiting textile mechanical anisotropy for fabric-based pneumatic actuators. *Soft Robot.* **5**, 662–674 (2018).
45. P. Polygerinos, Z. Wang, K. C. Galloway, R. J. Wood, C. J. Walsh, Soft robotic glove for combined assistance and at-home rehabilitation. *Rob. Auton. Syst.* **73**, 135–143 (2015).
46. H. Zhao, K. O'Brien, S. Li, R. F. Shepherd, Optoelectronically innervated soft prosthetic hand via stretchable optical waveguides. *Sci. Robot.* **1**, eaai7529 (2016).
47. R. Niiyama, X. Sun, C. Sung, B. An, D. Rus, S. Kim, Pouch motors: Printable soft actuators integrated with computational design. *Soft Robot.* **2**, 59–70 (2015).
48. H.-J. Kim, A. Kawamura, Y. Nishioka, S. Kawamura, Mechanical design and control of inflatable robotic arms for high positioning accuracy. *Adv. Robot.* **32**, 89–104 (2018).
49. P. H. Nguyen, W. Zhang, Design and computational modeling of fabric soft pneumatic actuators for wearable assistive devices. *Sci. Rep.* **10**, 9638 (2020).
50. A. Rajappan, B. Jumet, R. A. Shveda, C. J. Decker, Z. Liu, T. F. Yap, V. Sanchez, D. J. Preston, Logic-enabled textiles. *Proc. Natl. Acad. Sci. U.S.A.* **119**, e2202118119 (2022).
51. H. D. Yang, A. T. Asbeck, Design and characterization of a modular hybrid continuum robotic manipulator. *IEEE ASME Trans. Mechatron.* **25**, 2812–2823 (2020).
52. C. T. O'Neill, C. M. McCann, C. J. Hohimer, K. Bertoldi, C. J. Walsh, Unfolding textile-based pneumatic actuators for wearable applications. *Soft Robot.* **9**, 163–172 (2022).
53. X.-Y. Guo, W.-B. Li, Q.-H. Gao, H. Yan, Y.-Q. Fei, W.-M. Zhang, Self-locking mechanism for variable stiffness rigid–soft gripper. *Smart Mater. Struct.* **29**, 035033 (2020).
54. W. Park, S. Seo, J. Bae, A hybrid gripper with soft material and rigid structures. *IEEE Robot. Autom. Lett.* **4**, 65–72 (2019).
55. Y. Cui, X.-J. Liu, X. Dong, J. Zhou, H. Zhao, Enhancing the universality of a pneumatic gripper via continuously adjustable initial grasp postures. *IEEE Trans. Robot.* **37**, 1604–1618 (2021).
56. Y. Li, Y. Chen, Y. Yang, Y. Wei, Passive particle jamming and its stiffening of soft robotic grippers. *IEEE Trans. Robot.* **33**, 446–455 (2017).
57. Y. Wei, Y. Chen, T. Ren, Q. Chen, C. Yan, Y. Yang, Y. Li, A novel, variable stiffness robotic gripper based on integrated soft actuating and particle jamming. *Soft Robot.* **3**, 134–143 (2016).
58. G. B. Crowley, X. Zeng, H.-J. Su, A 3D printed soft robotic gripper with a variable stiffness enabled by a novel positive pressure layer jamming technology. *IEEE Robot. Autom. Lett.* **7**, 5477–5482 (2022).
59. K. C. Galloway, P. Polygerinos, C. J. Walsh, R. J. Wood, in *2013 16th International Conference on Advanced Robotics (ICAR)* (IEEE, 2013), pp. 1–6.
60. Y. Wang, Q. Xu, in *2018 IEEE International Conference on Mechatronics, Robotics and Automation (ICMRA)* (IEEE, 2018), pp. 157–161.
61. J. Zhou, S. Chen, Z. Wang, A soft-robotic gripper with enhanced object adaptation and grasping reliability. *IEEE Robot. Autom. Lett.* **2**, 2287–2293 (2017).
62. L. A. Al Abeach, S. Nefti-Meziani, S. Davis, Design of a variable stiffness soft dexterous gripper. *Soft Robot.* **4**, 274–284 (2017).
63. Y. Fei, J. Wang, W. Pang, A novel fabric-based versatile and stiffness-tunable soft gripper integrating soft pneumatic fingers and wrist. *Soft Robot.* **6**, 1–20 (2019).
64. L. Li, F. Xie, T. Wang, G. Wang, Y. Tian, T. Jin, Q. Zhang, Stiffness-tunable soft gripper with soft-rigid hybrid actuation for versatile manipulations. *Soft Robot.* **9**, 1108–1119 (2022).
65. A. Lotfiani, H. Zhao, Z. Shao, X. Yi, Torsional stiffness improvement of a soft pneumatic finger using embedded skeleton. *J. Mech. Robot.* **12**, 011016 (2020).
66. T. Sun, Y. Chen, T. Han, C. Jiao, B. Lian, Y. Song, A soft gripper with variable stiffness inspired by pangolin scales, toothed pneumatic actuator and autonomous controller. *Robot. Comput. Integr. Manuf.* **61**, 101848 (2020).
67. M. Wu, X. Zheng, R. Liu, N. Hou, W. H. Afridi, R. H. Afridi, X. Guo, J. Wu, C. Wang, G. Xie, Glowing sucker octopus (*Stauroteuthis syrtensis*)-inspired soft robotic gripper for underwater self-adaptive grasping and sensing. *Adv. Sci.* **9**, 2104382 (2022).
68. Z. Wu, X. Li, Z. Guo, A novel pneumatic soft gripper with a jointed endoskeleton structure. *Chin. J. Mech. Eng.* **32**, 78 (2019).
69. H. Lee, N. Oh, H. Rodrigue, Expanding pouch motor patterns for programmable soft bending actuation: Enabling soft robotic system adaptations. *IEEE Robot. Autom. Mag.* **27**, 65–74 (2020).
70. M. Fatahillah, N. Oh, H. Rodrigue, A novel soft bending actuator using combined positive and negative pressures. *Front. Bioeng. Biotechnol.* **8**, 472 (2020).
71. B. Calli, A. Walsman, A. Singh, S. Srinivasa, P. Abbeel, A. M. Dollar, Benchmarking in manipulation research: Using the Yale-CMU-Berkeley object and model set. *IEEE Robot. Autom. Mag.* **22**, 36–52 (2015).
72. X. Shi, Y. Zuo, P. Zhai, J. Shen, Y. Yang, Z. Gao, M. Liao, J. Wu, J. Wang, X. Xu, Q. Tong, B. Zhang, B. Wang, X. Sun, L. Zhang, Q. Pei, D. Jin, P. Chen, H. Peng, Large-area display textiles integrated with functional systems. *Nature* **591**, 240–245 (2021).
73. W. Yan, G. Noel, G. Loke, E. Meiklejohn, T. Khudiyev, J. Marion, G. Rui, J. Lin, J. Cherston, A. Sahasrabudhe, J. Wilbert, I. Wicaksono, R. W. Hoyt, A. Missakian, L. Zhu, C. Ma, J. Joannopoulos, Y. Fink, Single fibre enables acoustic fabrics via nanometre-scale vibrations. *Nature* **603**, 616–623 (2022).
74. Z. Yang, Z. Zhai, Z. Song, Y. Wu, J. Liang, Y. Shan, J. Zheng, H. Liang, H. Jiang, Conductive and elastic 3D helical fibers for use in washable and wearable electronics. *Adv. Mater.* **32**, 1907495 (2020).
75. C. Wielgosz, J.-C. Thomas, Deflections of inflatable fabric panels at high pressure. *Thin-Walled Struct.* **40**, 523–536 (2002).
76. R. Comer, S. Levy, Deflections of an inflated circular-cylindrical cantilever beam. *AIAA J* **1**, 1652–1655 (1963).
77. M. Stein, J. M. Hedgepeth, *Analysis of Partly Wrinkled Membranes* (National Aeronautics and Space Administration, 1961).
78. J. Hutchinson, Shear coefficients for Timoshenko beam theory. *J. Appl. Mech.* **68**, 87–92 (2001).

Acknowledgments: We thank Y. Lu, Z. Lu, S. Zhang, and J. Li (SJTU) for participations in the grasping tests and I. Lu (Imperial College London/FDU) for the discussions about the robotic gripper. H.J. and Z.Z. also acknowledge the Research Center for Industries of the Future (RCIF) at Westlake University and Westlake Education Foundation for supporting this work. **Funding:** This work was supported by the National Key Research and Development Program of China (grant 2019YFA0709001) and the National Natural Science Foundations of China (grants 52205031, 52022056, and 51875334). **Author contributions:** Conceptualization: Z.Z., G.C., and H.J. Methodology: Z.Z., Y.L., G.C., Q.W., and H.J. Investigation: Z.Z., Y.L., G.C., H.W., and H.J. Visualization: Z.Z., Y.L., and Q.W. Writing—review and editing: Z.Z., Y.L., G.C., and H.J. **Competing interests:** The authors declare that they have no competing interests. **Data and materials availability:** All data needed to evaluate the conclusions in the paper are present in the paper and/or the Supplementary Materials.

Submitted 4 December 2022
Accepted 14 March 2023
Published 12 April 2023
10.1126/sciadv.adg1203